Critical adsorption at silicon surfaces in binary liquid mixtures

J.-H. J. Cho and B. M. Law
Condensed Matter Laboratory, Department of Physics, Kansas State University, Manhattan, Kansas 66506-2601, USA
(Received 14 July 2005; published 5 October 2005)

In critical binary liquid mixtures the preferential adsorption that occurs at liquid-vapor or liquid-solid surfaces is expected to be described by a *universal* surface scaling function. In this paper, we show that aniline strongly adsorbs at an oxide-coated Si wafer surface from a critical mixture of aniline + cyclohexane where this solid-liquid adsorption can be described by the *same* universal function found at liquid-vapor surfaces. For a tetrabromoethane + *n*-dodecane critical mixture the *n*-dodecane adsorption on an alkylsilane coated Si wafer cannot be described by previously determined adsorption functions. We speculate that this discrepancy is caused by chemical heterogeneities at the alkylsilane surface due to differing surface distributions of —CH_3 and —CH_2— groups within the silane layer.

DOI: 10.1103/PhysRevE.72.041601 PACS number(s): 64.60.Fr, 68.08.−p, 68.35.Rh

I. INTRODUCTION

Scientists have been attempting to understand the processes of adsorption at surfaces for more than a century [1,2]. For a gaseous system, the thickness of an adsorbed layer at a solid surface will in general depend upon the temperature, pressure, and surface potential. A direct one-to-one correspondence can be made between this gaseous adsorption process and the preferential adsorption that occurs at the liquid-vapor or liquid-solid surface of a binary *AB* liquid mixture; hence, study of one provides information about the other system. In this paper, we study the preferential adsorption that occurs at the surfaces of critical binary *AB* liquid mixtures. Near the critical point of the liquid mixture the adsorption actually *simplifies* because, in this case, the relevant length scale of the correlation length ξ diverges and becomes much larger than a molecular size, hence, molecular details become unimportant and the adsorption is described by *universal* surface behavior [3].

For example, let's consider the liquid-vapor surface of a critical binary liquid mixture. If the surface tension difference between the two components is sufficiently large, $\sigma_B \ll \sigma_A$, then this surface will be completely saturated by component *B*, a situation which is frequently called strong adsorption. The local composition $v(z)$, therefore, varies with depth z from pure *B* at the surface ($z=0$) to the mixture's critical composition in the bulk ($z\to\infty$). This surface variation can be described by a universal surface scaling function $P(x)$ of the dimensionless depth $x=(z+z_e)/\xi$, where z_e is an extrapolation length [4]. Much theoretical and experimental work has been expended over the last 25 years in deducing the precise form for this universal function. $P(x)$ crosses over from power law behavior at $x\ll 1$ [5] to exponential behavior at $x\gg 1$ (Fig. 1) [4]. A complication arises if $\sigma_B \simeq \sigma_A$. In this competitive or weak adsorption regime, the surface is now no longer saturated by a single component. The surface composition then becomes a function of the surface tension difference $\Delta\sigma=\sigma_A-\sigma_B$ where the dimensionless parameter $y=h_1 t^{-\Delta_1}$ controls this behavior [6,7]. Here $h_1\sim\Delta\sigma$ is a surface field, while the surface critical exponent $\Delta_1=0.464$ [8]. This weak adsorption behavior is described by another universal surface scaling function $G(x,y)$ of the two variables x and y where, in the limit of large y, $G(x,y\to\infty)=P(x)$. The function $G(x,y)$ exhibits a peak as a function of z (Fig. 1), where the small z behavior is primarily influenced by the surface field h_1; but with increasing z, this crosses over to $P(x)$ behavior determined by the bulk thermodynamics of the mixture which is governed by the correlation length ξ. Another complication arises if either of the components is highly polar. In this case, the local surface orientational order of the polar component can vary with dimensionless depth x due to the interaction between the dipole and its image dipole when in the vicinity of a surface [9]. Here, we only consider nonpolar or weakly polar critical mixtures in order to eliminate this complication.

Recently a universal form for P was determined which described the liquid-vapor ellipsometric critical adsorption behavior for five different critical mixtures [10,11]. Subsequently a form for G was determined by studying the homologous series of critical liquid mixtures *n*-alkane + methyl format [12,13]. As the *n*-alkane chain length increased, $\Delta\sigma$ changed sign, and hence, the surface preference changed

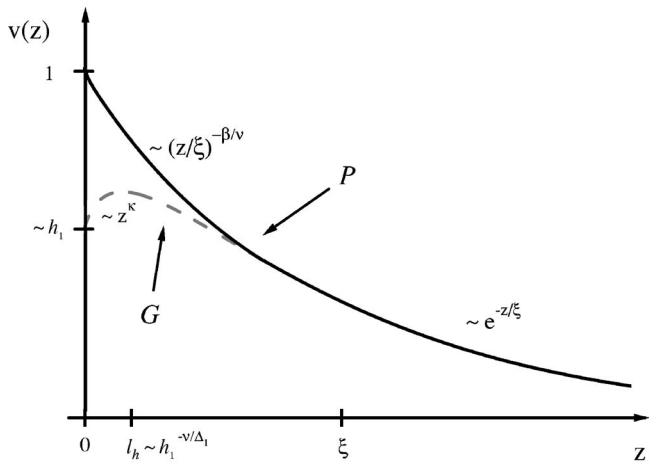

FIG. 1. Schematic diagram of strong P (solid line) and weak G (dashed line) adsorption as a function depth z. The critical exponent $\kappa=(\Delta_1-\beta)/\nu\approx 0.21$.

from *n*-alkane to methyl format with a consequent change in surface behavior. These universal functions, P and G, were determined from experimental data collected at the *liquid-vapor* surface of critical mixtures. An open question which has never been addressed is: Do the same universal functions P and G also describe the adsorption behavior at *liquid-solid* surfaces? This is an important question because solid surfaces are technologically more important than liquid-vapor surfaces. Solid surfaces are also in general more complex than liquid-vapor surfaces. Solid surfaces may be heterogeneous and are often much rougher than liquid-vapor surfaces. In this paper, we consider the adsorption behavior of critical binary liquid mixtures in the single liquid phase region against molecularly smooth Si wafers in order to investigate this surface universality.

This paper is set out as follows. The universal functions P and G determined at the liquid-vapor surface are described in Sec. II. Section III compares experimental ellipsometric measurements of the adsorption at critical mixture/solid surfaces with these universal functions. This publication concludes with a summary of our results in Sec. IV.

II. SURFACE SCALING FUNCTIONS FOR CRITICAL ADSORPTION

For strong adsorption, the local volume fraction of the adsorbed component B is described by

$$v(z) = v_c + Mt^{\beta}P(x), \tag{1}$$

where

$$x = (z + z_e)/\xi \tag{2}$$

and the correlation length

$$\xi = \xi_o t^{-\nu}. \tag{3}$$

Here v_c is the critical volume fraction, $t=(T-T_c)/T_c$ is the reduced temperature relative to the mixture's critical temperature T_c, Mt^{β} describes the shape of the binary liquid coexistence curve where the critical exponents $\beta=0.3255$ and $\nu=0.630$ [14]. ξ_o and M are system dependent amplitudes. A particular model for $P(x)$ was determined from experimental data in Ref. [10]. At small x, the universal function $P(x)$ has power law behavior [15]

$$P(x) = cx^{-\beta/\nu} + c_1 x^{(1-\beta)/\nu}, \quad 0 < x \leqslant x_o, \tag{4}$$

which crosses over to exponential decay [4,16]

$$P(x) = P_{\infty}e^{-x} + P_1 e^{-2x}, \quad x \geqslant x_o \tag{5}$$

at large x. The amplitudes c, c_1, P_{∞}, P_1, and the crossover point x_o are universal. Constraints on the continuity of P and its first derivative at x_o, continuity of $v(z)$ at T_c, and fits to experimental data determined the values for these parameters given in Table I; this model for P was called the $P1$ model in Ref. [10]. The extrapolation length z_e cuts off the power law divergence at very small x so that the surface is completely saturated by component B [i.e., $v(0)=1$], which implies from Eqs. (1)–(4) that [17]

TABLE I. Critical adsorption scaling function parameters.

Parameters		Critical Exponents	
c	0.788	β	0.3255
c_1	−0.245	ν	0.630
P_{∞}	0.963	Δ_1	0.464
P_1	1.437		
x_o	1.15		

$$z_e \simeq \xi_o \left(\frac{1 - v_c}{Mc} \right)^{-\nu/\beta}. \tag{6}$$

In this formulation, once the system dependent parameters v_c, M, ξ_o, and T_c are known for a particular mixture, then $v(z)$ is completely specified.

The universal function $G(x,y)$ for weak adsorption is a perturbation about the $P(x)$ function because of the requirement that

$$G(x, y \to \infty) = P(x). \tag{7}$$

In Ref. [13], we have shown that

$$v(z) = v_c + Mt^{\beta}G(x,y), \tag{8}$$

where

$$G(x,y) = P(x)Z(x,y), \tag{9}$$

$$Z(x,y) = (1 - e^{-\varsigma})^{\Delta_1/\nu}, \tag{10}$$

$$\varsigma \equiv xy^{\Delta_1/\nu} \text{ and } y = h_1 t^{-\Delta_1} \tag{11}$$

provide an excellent description of experimental liquid-vapor critical adsorption data in the single phase region for the homologous critical mixture *n*-alkane + methyl format. In this homologous series, the surface tension difference $\Delta\sigma$ changes sign with increasing *n*-alkane chain length, thus, we are in the region of weak adsorption. These equations are in conformity with theoretical expectations [7]. At the liquid-vapor interface, the surface field h_1 is related to $\Delta\sigma$ via

$$h_1 = \frac{(\sigma_A - \sigma_B)l_{\sigma}^2}{k_B T_c}, \tag{12}$$

where $k_B T_c$ is the thermal energy, while l_{σ} is an additional system dependent length scale associated with the surface field, which will be characteristic of a particular homologous system. For room temperature critical mixtures, one must consider the weak adsorption G function when $\Delta\sigma \leqslant 6$ mN/m [11].

It is not so obvious how to interpret h_1 for solid surfaces. In this paper, h_1 is treated as an adjustable parameter.

III. CRITICAL ADSORPTION EXPERIMENTS

We consider two different types of systems in this paper. In the first system, a critical mixture of aniline + cyclohexane (AC) is studied against a native oxide-coated Si wafer.

TABLE II. Critical mixture materials parameters.

	ε[a]	M	ξ_o(nm)	v_c[b]	$T_c(^0C)$	ε_1[c]
aniline (A)	2.516	1.03[d]	2.3[d]	0.59	33.007	2.22
cyclohexane (C)	2.035					
tetrabromoethane (T)	2.680	0.869[e]	2.9[e]	0.45	37.347	2.36
n-dodecane (D)	2.019					

[a]Optical dielectric constant ε at 20 °C from the manufacturer's data sheet.
[b]Critical volume fraction v_c of cyclohexane (dodecane) for the AC (TD) mixture.
[c]Optical dielectric constant of the critical mixture.
[d]From Ref. [29].
[e]From Ref. [11].

Aniline is weakly polar with a dipole moment of 1.55D and cyclohexane is nonpolar, hence, no additional complications from dipole-image dipole interactions are expected. The lone electron pair on the nitrogen atom will cause the aniline to hydrogen bond to the hydroxyl groups (-OH) on the oxide surface. Therefore, this system is expected to fall into the category of *strong* aniline adsorption against a Si wafer and be described by the $P(x)$ function.

In the second system, the nonpolar critical mixture 1,1,2,2-tetrabromoethane + n-dodecane (TD) is studied against an alkylsilane self-assembled monolayer-coated Si wafer. Alkylsilanes are technologically important and are often used to control the wettability of Si wafers. In this study, we have used a hexadecyltrichlorosilane which possesses a methyl end group (—CH_3). This surface most closely resembles the n-dodecane component of the mixture, therefore, this component is expected to preferentially adsorb against the wafer.

Aniline and n-dodecane were purchased from Aldrich, cyclohexane was purchased from Fisher, while tetrabromoethane was purchased from Fluka. All of the chemicals were used without any further purification. They had a specified purity of 99+%, except tetrabromoethane which had purity of 98+%. Teflon 0.5 μm Millipore filters were used to remove particulates. For each of the critical binary mixtures, many system dependent parameters must be independently determined before an accurate comparison can be made between the theory and the experiment. Table II lists relevant liquid and liquid mixture parameters.

Our ellipsometric sample cell is of simple construction. It is composed of a chemically resistant Pyrex cylinder of inner diameter ~3 cm, total length 10 cm with threaded glass necks (Ace Glass Cat. No. 7644-25) at both ends. Each end was sealed by screwing a Teflon bushing (Ace Glass Cat. No. 7506-35) against a Teflon cap, which compressed a Teflon-coated O-ring between the glass wall and cap. The glass cell was initially washed well, glass etched using a solution of 35% HNO_3, 5% HF, and 60% distilled water by volume, rinsed well with double distilled deionized water, and finally dried at ~120 °C overnight. All other teflon components constituting the cell were cleaned in an ultrasonic bath for 20 min using acetone and then ethanol before drying overnight at ~120 °C.

The (100) Si wafers of 3 mm thickness and 1–10 Ω cm resistivity were purchased from Semiconductor Processing Company. They were factory polished on one side only and possessed a ~2 nm thick native oxide coating. The wafers were carefully cut using a diamond saw to a size of ~2.5 $\times$4 nm^2 for installation in the sample cell. The wafers were initially cleaned by agitating in piranha solution (30% of a 30% solution of H_2O_2 and 70% H_2SO_4) for 20 min at 120 °C, rinsed thoroughly with distilled, deionized water before drying with a hot air blower inside a laminar flow clean bench. Alkylsilane layers were deposited by immersing a wafer in a silane solution composed of 0.5 ml n-hexadecyltrichlorosilane (United Chemical Technologies Corp.) in 30 ml of n-hexadecane (Aldrich) for 2 h at 18 °C inside a low humidity closed atmospheric bag [18]. The wafer was then prerinsed for 5 min and finally sonicated with warm chloroform for 20 min in order to remove any silane clusters which may have formed on the surface. A contact mode atomic force microscope image indicates that the uncoated wafer has a surface roughness of ~0.14 nm, while the silane-coated silicon wafer has a surface roughness of ~0.36 nm (Fig. 2). This later image was taken at the end of the ellipsometry experiment after this Si wafer had been immersed in the TD mixture for approximately one month. The contact angle of water was ~100° on the silane-coated hydrophobic Si wafer. Each Si substrate was positioned via a slot in the Teflon cap so that its polished surface was situated at the center of the sample cell.

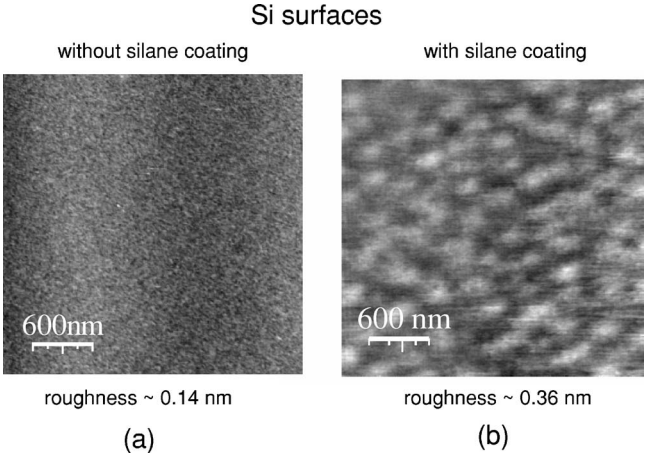

FIG. 2. Contact mode atomic force microscope images of silicon surfaces (a) without and (b) with a silane film.

Temperature control of the critical mixture + Si substrate within the sample cell was achieved via a two stage oven composed of an inner resistively heated shell and an outer water cold shell of similar construction to Ref. [19]. Thermal gradients along the length of the sample cell were less than ~1 mK/cm, while short and long term thermal stabilities are, respectively, ~0.1 mK over 4 h and ~1 mK per day. The critical temperature of each mixture was measured *in situ* to within a few mK by observation of the phase separation behavior.

A custom-made computer controlled phase-modulated ellipsometer possessing a horizontal plane of incidence was used to measure the critical adsorption behavior as a function of temperature. The construction and operation of our phase-modulated ellipsometer is similar to the description in Ref. [20]. A HeNe laser, with wavelength $\lambda = 632.8$ nm, is used as the light source where, after appropriate polarization and phase modulation, the reflected beam from the liquid-solid surface provides a measurement of the ellipticity,

$$\bar{\rho} \equiv \mathrm{Im}(r_p/r_s)|_{\theta_B}, \tag{13}$$

at the Brewster angle (θ_B). Here, r_p and r_s are the complex reflection amplitudes for polarizations parallel (p) and perpendicular (s) to the plane of incidence and the Brewster angle is operationally defined by that angle of incidence where

$$\mathrm{Re}(r_p/r_s)|_{\theta_B} = 0. \tag{14}$$

In the ellipsometric measurement at each temperature, $\bar{\rho}$ and T measurements were collected every 30 min over a period of from 10 to 24 h to ensure thermal and diffusive equilibrium. The averaged equilibrium data was then considered for further analysis. In all measurements, the temperature was decreased in successive steps so that gravity assisted the phase separation process.

The ellipticity $\bar{\rho}$ versus the reduced temperature t for the two systems in the single phase region is shown in Fig. 3. For AC, $\bar{\rho}$ increases as one approaches T_c, while the converse occurs for TD, namely, $\bar{\rho}$ decreases as one approaches T_c. A qualitative understanding of this trend can be obtained from the Drude equation [21], which is valid for sufficiently thin layers relative to the wavelength of light λ,

$$\bar{\rho}(t) = \frac{\pi}{\lambda}\frac{\sqrt{\varepsilon_1+\varepsilon_2}}{\varepsilon_1-\varepsilon_2}\int_{-\infty}^{\infty}\frac{[\varepsilon(z,t)-\varepsilon_1][\varepsilon(z,t)-\varepsilon_2]}{\varepsilon(z,t)}dz \tag{15}$$

$$\simeq \bar{\rho}_c(t) + \bar{\rho}_{BG}. \tag{16}$$

The ellipsometric beam is incident through the critical mixture with optical dielectric constant ε_1 given in Table I while $\varepsilon_2 \equiv \varepsilon_{\mathrm{Si}} = 15.07$ [22]. $\varepsilon(z,t)$ describes the variation in the optical dielectric constant as a function of depth z and reduced temperature t. To a good approximation, $\bar{\rho}$ can be separated into a critical component $\bar{\rho}_c(t)$ within the liquid phase at $z \geqslant 0$ and a temperature independent background term $\bar{\rho}_{BG}$ within the substrate at $z < 0$. In separating these two contributions, the approximations $\varepsilon(z,t) \simeq \varepsilon_1$ and $|\varepsilon(z,t)-\varepsilon_1| \ll |\varepsilon_1-\varepsilon_2|$ have been used, which leads to

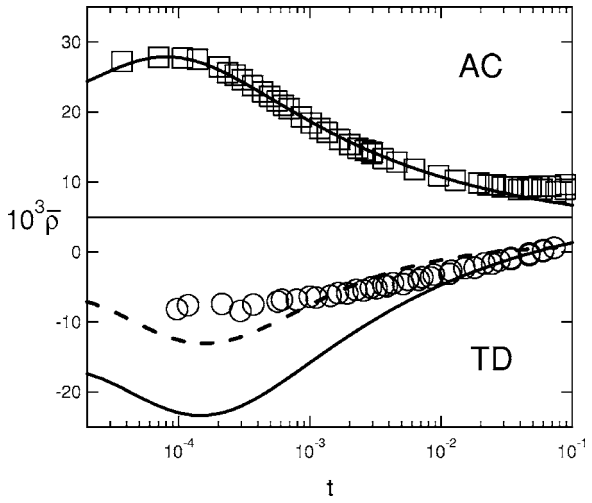

FIG. 3. Comparison of the ellipticity $\bar{\rho}$ calculated for strong (solid line) and weak adsorption (dashed line) with experimental data for the AC (squares) and TD (circles) mixtures in the single liquid phase region.

$$\bar{\rho}_c(t) \simeq \frac{\pi}{\lambda}\frac{\sqrt{\varepsilon_1+\varepsilon_2}}{\varepsilon_1}\int_0^{\infty}[\varepsilon(z,t)-\varepsilon_1]dz. \tag{17}$$

$\bar{\rho}_{BG}$ dominates the $\bar{\rho}$ signal at very large $t \sim 0.1$. According to Fig. 3, $\bar{\rho}_c(t)$ must be positive (negative) for AC (TD) in order to give the trends shown. This requires that $\varepsilon(z,t) > \varepsilon_1$ [$\varepsilon(z,t) < \varepsilon_1$] for AC (TD). Therefore, from Table II, aniline (A) preferentially adsorbs against the Si wafer in the mixture AC while n-dodecane (D) preferentially adsorbs against the Si wafer in the mixture TD. These preferential adsorptions qualitatively agree with the expectations discussed earlier.

As mentioned above, the Drude equation is only valid for very thin layers which occur at large t. In general, to compare a specific model for $\varepsilon(z,t)$ with $\bar{\rho}$ data, one must numerically solve Maxwell's equations for r_p and r_s [23,24] and then calculate $\bar{\rho}$ from Eq. (13). To accomplish such a comparison, one must have an accurate model of the oxide and alkylsilane layers. Independent measurements [25] indicate that the oxide had a thickness $d_{ox} = 1.9$ nm and optical dielectric constant $\varepsilon_{ox} = 2.67$, while for the alkylsilane $d_{silane} = 2.0$ nm and $\varepsilon_{silane} = 2.43$. One must also relate the local volume fraction $v(z)$, which occurs in the theory (Sec. II) to the local optical dielectric constant $\varepsilon(z) \equiv \varepsilon(z,t)$ used in Maxwell's equations. This is accomplished via the two-component Clausius-Mossotti equation [26],

$$f[\varepsilon(z)] = v(z)f(\varepsilon_B) + [1-v(z)]f(\varepsilon_A), \tag{18}$$

where the function

$$f(\epsilon) = \frac{\epsilon-1}{\epsilon+2}, \tag{19}$$

ε_A and ε_B are the optical dielectric constants of the pure components (Table II), and we have neglected any volume changes due to mixing of the two components (which normally only amount to corrections of order ~1–2%). In Eq. (18), component B is assumed to adsorb against the Si wafer.

In Fig. 3, the ellipsometric $\bar{\rho}$ data for the *AC* critical mixture adsorbing against the oxide-coated Si wafer is shown. There is excellent agreement between the strong adsorption model (solid line) for aniline adsorbing against the surface and experimental data (squares). The variation in the shape of $\bar{\rho}$ with t originates from the variation of $v(z)$ with t. The oxide layer accounts for much of the background ellipticity $\bar{\rho}_{BG} \simeq 0.01$. In this comparison between theory and experiment, there should be no adjustable parameters; however, in obtaining the optimal fit, we have allowed for a small shift in the background of order ~ 0.002. This shift merely moves the whole curve vertically without changing its shape. This small change in the background could be caused by the surface roughness of the silicon wafer or by other noncritical effects.

In the lower part of Fig. 3, we show the variation of $\bar{\rho}$ with t for *TD* adsorbing against an alkylsilane-coated Si wafer. Neither strong (solid line) nor weak adsorption (dashed line) of *n*-dodecane against the surface can explain the experimental data, (circles). In comparing these models with experimental data, the background $\bar{\rho}_{BG}$ was shifted slightly (~ 0.005), while the surface field h_1 was treated as an adjustable parameter for weak adsorption where the best fit occurred for $h_1 \simeq 0.008$, which corresponds to a length scale for the position of the peak in Fig. 1 of $l_h (\equiv \xi_o h_1^{-\nu/\Delta_1}) = 20$ nm [13]. We suspect that the poor agreement between theory and experiment might be due to slight chemical heterogeneities in the silane-coated Si wafer surface as suggested by the textual differences on length scales of ~ 100 nm and the increased surface roughness exhibited in Fig. 2(b). These features could be caused by slight local differences in the silane surface densities leading to varying surface distributions of $-CH_3$ and $-CH_2-$ groups within the silane layer. According to Zisman [27], these two surface groups have rather different "critical surface tensions" of, respectively, 24 and 31 mN/m, which will lead to differing preferential adsorption properties. This experimental data might, therefore, be better described in terms of critical adsorption in the presence of a random surface field h_1 [28].

IV. SUMMARY

In prior work, the critical adsorption behavior of a number of critical binary liquid mixtures, including *AC* and *TD*, have been studied at the liquid-vapor surface for both strong [10,11] and weak [12,13] surface field. At the noncritical liquid-vapor surface, the surface field is controlled by the surface tension difference $\Delta\sigma$ between the two components of the binary liquid mixture. If this surface tension difference is large ($|\Delta\sigma| \gg 6$ mN/*m*), the liquid-vapor interface is in the strong critical adsorption regime [11], which is described by the $P(x)$ surface scaling function [Eqs. (4) and (5)]. The liquid-vapor surface is saturated by the component which possesses the lowest surface energy. The $P(x)$ surface scaling function for strong adsorption crosses over into the weak surface scaling function $G(x,y)$ [Eqs. (9)–(11)] in the limit of small surface field where the surface tension difference is relatively small ($|\Delta\sigma| \lesssim 6$ erg/cm^2). The surface is now no longer saturated by a single component.

These same universal functions $P(x)$ and $G(x,y)$ found at the liquid-vapor surface of critical mixtures are expected to describe the adsorption behavior at liquid-solid surfaces of critical mixtures. Indeed, we find that the strong adsorption surface scaling function $P(x)$ provides an excellent description of the critical adsorption behavior for aniline adsorbing on an oxide-coated Si wafer surface from a critical mixture of aniline + cyclohexane (Fig. 3, upper curve). By contrast with this very good agreement, poor agreement was found between theory and experiment for *n*-dodecane adsorbing against an alkylsilane coated Si wafer from a critical mixture of 1,1,2,2-tetrabromoethane + *n*-dodecane (Fig. 3, lower curve). Neither weak nor strong critical adsorption could explain the experimental data. We speculate that this discrepancy is caused by chemical heterogeneities within the alkylsilane layer due to differing surface distributions of $-CH_3$ and $-CH_2-$ groups leading to a locally varying preferential adsorption more characteristic of a randomly varying surface field [28].

This work was partially supported by the National Science Foundation through Grant No.DMR-0097119 and the Department of Energy through Grant No. DE-FG02-02ER46020.

[1] J. W. Gibbs, *The Collected Works of J. W. Gibbs* (Longmans, Green, New York, 1931).
[2] A. W. Adamson, *Physical Chemistry of Surfaces*, 4th ed. (Wiley, New York, 1982).
[3] H. W. Diehl, Int. J. Mod. Phys. B **11**, 3503 (1997).
[4] A. J. Liu and M. E. Fisher, Phys. Rev. A **40**, 7202 (1989).
[5] M. E. Fisher and P-G. de Gennes, C. R. Seances Acad. Sci., Ser. B **287**, 207 (1978).
[6] H. Au-Yang and M. E. Fisher, Phys. Rev. B **21**, 3956 (1980); Physica A **101**, 255 (1980).
[7] U. Ritschel and P. Czerner, Phys. Rev. Lett. **77**, 3645 (1996); A. Ciach and U. Ritschel, Nucl. Phys. B **489**, 653 (1997); P. Czerner and U. Ritschel, Physica A **237**, 240 (1997); A. Ciach, A. Maciolek, and J. Stecki, J. Chem. Phys. **108**, 5913 (1998).
[8] H. W. Diehl and M. Shpot, Nucl. Phys. B **528**, 595 (1998).
[9] J-H. J. Cho and B. M. Law, Phys. Rev. Lett. **89**, 146101 (2002); J-H. J. Cho and B. M. Law, Phys. Rev. E **67**, 031605 (2003).
[10] J. H. Carpenter, B. M. Law, and D. S. P. Smith, Phys. Rev. E **59**, 5655 (1999); J. H. Carpenter, J-H. J. Cho, and B. M. Law, Phys. Rev. E **61**, 532 (2000).
[11] J-H. J. Cho, B. M. Law, and K. Gray, J. Chem. Phys. **116**, 3058 (2002).
[12] J-H. J. Cho and B. M. Law, Phys. Rev. Lett. **86**, 2070 (2001).
[13] J-H. J. Cho and B. M. Law, Phys. Rev. E **65**, 011601 (2001).
[14] R. Guida and J. Zinn-Justin, J. Phys. A **31**, 8103 (1998); M.

Campostrini, A. Pelissetto, P. Rossi, and E. Vicari, Phys. Rev. E **60**, 3526 (1999).
[15] H. W. Diehl and M. Smock, Phys. Rev. B **47**, 5841 (1993); **48**, 6740(E) (1993).
[16] Z. Borjan and P. J. Upton, Phys. Rev. E **63**, 065102(R) (2001);; Z. Borjan, Ph.D. thesis, University of Bristol, 1999 (unpublished).
[17] D. S. P. Smith and B. M. Law, Phys. Rev. E **52**, 580 (1995).
[18] J. B. Brzoska, I. Ben Azouz, and F. Rondelez, Langmuir **10**, 4367 (1994).
[19] M. Brown, S. Uran, B. Law, L. Marschand, L. Lurio, I. Kuzmenko, and T. Gog, Rev. Sci. Instrum. **75**, 2536 (2004).
[20] D. Beaglehole, Physica B & C **100**, 163 (1980).
[21] P. K. L. Drude, *The Theory of Optics* (Dover, New York, 1959), p. 292.
[22] D. F. Edwards, in *Handbook of Optical Constants of Solids*, edited by E. D. Palik (Academic, Orlando, 1985), p. 547.
[23] B. M. Law and D. Beaglehole, J. Phys. D **14**, 115 (1981).
[24] M. Born and E. Wolf, *Principle of Optics* (Pergamon, Oxford, 1980), Sec. 1.6.
[25] Y. Takata, J-H. J. Cho, and B. M. Law (unpublished).
[26] R. F. Kayser, Phys. Rev. B **34**, 3254 (1986).
[27] W. A. Zisman Adv. Chem. Ser. **43**, 1 (1964).
[28] G. Forgacs, R. Lipowsky, and Th. M. Nieuwenhuizen, in *Phase Transitions and Critical Phenomena*, edited by C. Domb and J. L. Lebowitz (Academic, London, 1991), Vol. 14, p. 135; M. Pleimling, F. A. Bagamery, L. Turban, and F. Igloi, J. Phys. A **37**, 8801 (2004).
[29] D. S. P. Smith, B. M. Law, M. Smock, and D. P. Landau, Phys. Rev. E **55**, 620 (1997).